Atmospheric Research 204 (2018) 1–11

Contents lists available at ScienceDirect

Atmospheric Research

journal homepage: www.elsevier.com/locate/atmosres

Spatial-temporal changes of maximum and minimum temperatures in the Wei River Basin, China: Changing patterns, causes and implications

Saiyan Liu[a], Shengzhi Huang[a,*], Yangyang Xie[a], Qiang Huang[a], Guoyong Leng[b], Beibei Hou[a], Ying Zhang[a], Xiu Wei[a]

[a] State Key Laboratory of Eco-hydraulics in Northwest Arid Region of China, Xi'an University of Technology, Xi'an 710048, China
[b] Key Laboratory of Water Cycle and Related Land Surface Processes, Institute of Geographic Sciences and Natural Resources Research, Chinese Academy of Sciences, Beijing 100101, China

ARTICLE INFO

Keywords:
Annual maximum temperature
Annual minimum temperature
Cloud model
Cross wavelet analysis
Atmospheric circulation anomaly
Precipitation extremes

ABSTRACT

Due to the important role of temperature in the global climate system and energy cycles, it is important to investigate the spatial-temporal change patterns, causes and implications of annual maximum (Tmax) and minimum (Tmin) temperatures. In this study, the Cloud model were adopted to fully and accurately analyze the changing patterns of annual Tmax and Tmin from 1958 to 2008 by quantifying their mean, uniformity, and stability in the Wei River Basin (WRB), a typical arid and semi-arid region in China. Additionally, the cross wavelet analysis was applied to explore the correlations among annual Tmax and Tmin and the yearly sunspots number, Arctic Oscillation, Pacific Decadal Oscillation, and soil moisture with an aim to determine possible causes of annual Tmax and Tmin variations. Furthermore, temperature-related impacts on vegetation cover and precipitation extremes were also examined. Results indicated that: (1) the WRB is characterized by increasing trends in annual Tmax and Tmin, with a more evident increasing trend in annual Tmin, which has a higher dispersion degree and is less uniform and stable than annual Tmax; (2) the asymmetric variations of Tmax and Tmin can be generally explained by the stronger effects of solar activity (primarily), large-scale atmospheric circulation patterns, and soil moisture on annual Tmin than on annual Tmax; and (3) increasing annual Tmax and Tmin have exerted strong influences on local precipitation extremes, in terms of their duration, intensity, and frequency in the WRB. This study presents new analyses of Tmax and Tmin in the WRB, and the findings may help guide regional agricultural production and water resources management.

1. Introduction

According to the latest Intergovernmental Panel on Climate Change (IPCC) report, the global average temperature increased by approximately 0.72 °C during the period of 1951–2012, due to the combined effects of climate change and human-induced greenhouse gas emissions (IPCC, 2013). The rising temperature trends have been accompanied by the increasing maximum temperature (Tmax) and minimum temperature (Tmin) across the globe (Kruger and Sekele, 2013; Fonseca et al., 2015). Since temperature plays a crucial role in the global climate system and energy cycles, more frequent occurrences of Tmax and Tmin are likely to significantly impact hydrology, agriculture, ecosystems, and many aspects of human life, such as mortality, morbidity, health, and comfort (Trenberth, 2011; Wang et al., 2013; Huang et al., 2014a; Leng et al., 2015; Ngo and Horton, 2015; Liu et al., 2017). Furthermore, there is growing evidence that Tmax and Tmin may become more extreme and occur even more frequently in the future (Orlowsky and Seneviratne, 2012; Wang et al., 2013; Fonseca et al., 2015). Therefore, investigations of Tmax and Tmin have been strongly utilized to improve our understanding of climate change, the scientific prevention and mitigation of disasters, and water resources management.

To date, numerous studies focused on Tmax and Tmin have been performed globally and regionally. For example, on the global scale, Donat and Alexander (2012) concluded, based on daily global observations, that changes in daily Tmax and Tmin were the result of a combination of changes in their mean, variance and skewness. At the regional scale, an increasing trend in Tmax was mainly observed in the Gobi Desert of Mongolia, while a significantly increasing trend in Tmin has been confirmed across the entirety of Mongolia (Dashkhuu et al., 2014). In Australia, changes in Tmax and Tmin were identified, when statistically significant trends in Tmax showed marked regional and seasonal variations, but the increase in Tmin typically exceeded the increase in Tmax (Jakob and Walland, 2016). In Pakistan, Tmin showed clearly positive trends in the pre-monsoon season and on the annual

* Corresponding author at: State Key Laboratory Base of Eco-Hydraulic Engineering in Arid Area, Xi'an University of Technology, Xi'an 710048, China.
E-mail address: huangshengzhi@xaut.edu.cn (S. Huang).

https://doi.org/10.1016/j.atmosres.2018.01.006
Received 19 May 2017; Received in revised form 5 January 2018; Accepted 5 January 2018
Available online 02 February 2018

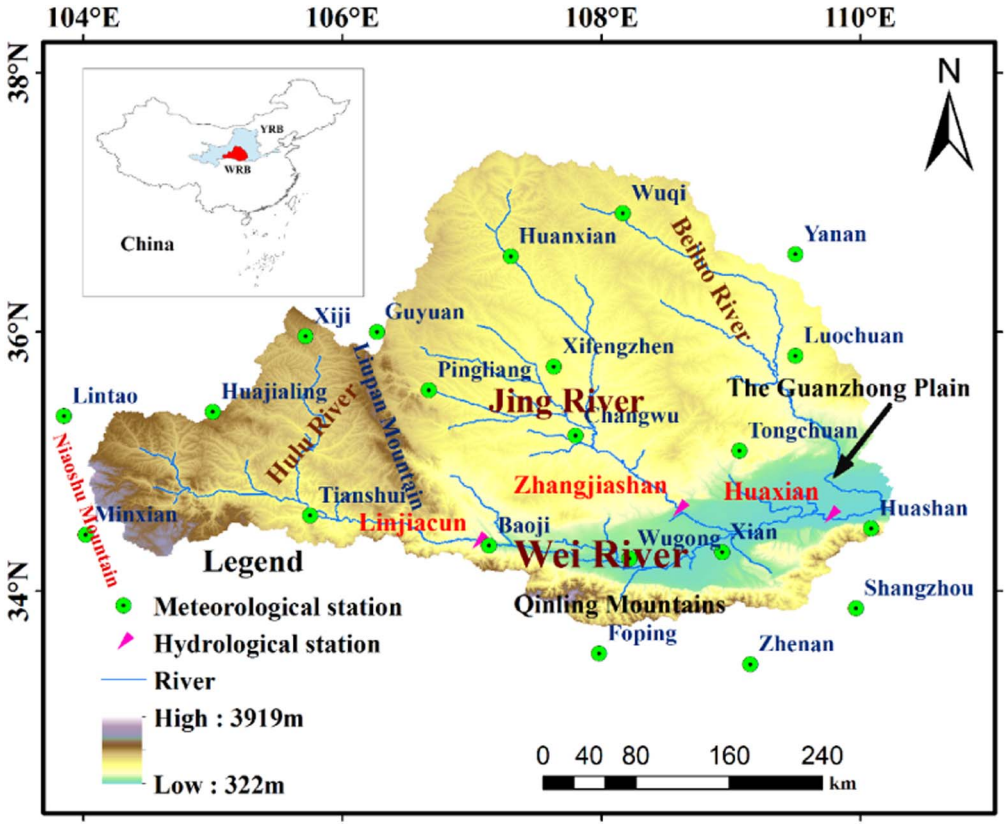

Fig. 1. Location of the WRB and relevant hydro-meteorological stations.

scale, while Tmax increased faster than Tmin in all seasons and on the annual scale in the northern areas of the country. Similar changes in Tmin and Tmax were also observed in China with pronounced magnitude and regional differences (Zhou and Ren, 2011; Yu and Li, 2015; Jiang et al., 2016; Zhang et al., 2017).

These previous studies provide key insights towards understanding the changing characteristics of Tmax and Tmin at various temporal and regional scales. However, most of the investigations thus far have been focused on variations of mean, variance, and trends in temperature extremes, which only reveal certain aspects of Tmax and Tmin characteristics. To more fully represent the uncertainties in modelling these phenomena, Li et al. (1998, 2009) developed a cognitive model called "the Cloud model", based on the fuzzy set theory and probability measures. It has been proven to be robust in estimating the uniformity and stability of qualitative concepts and quantitative data (Huang et al., 2015a; Zhu et al., 2016). Thus, the Cloud model is now widely used in data mining, image processing, uncertainty reasoning, etc. (Li et al., 1998; Yang and Chen, 2007; Wang and Deng, 2007). However, it has rarely been used in the investigation of spatial-temporal changes in annual Tmax and Tmin. Since there are many uncertainties in annual Tmax and Tmin, it is important to adopt the Cloud model to fully and accurately analyze the spatial-temporal change patterns in annual Tmax and Tmin. This offers a new approach and quantitative measure for assessing the stability and uniformity of annual Tmax and Tmin series.

Many factors affect temperature variations, such as solar activity (Kristoufek, 2016), large-scale atmospheric circulation patterns (Nyeko-Ogiramoi et al., 2013; Zhong et al., 2017), and topography (Jiang et al., 2016). Recently, the role of soil moisture (SM) in the occurrence of temperature extremes in transitional climate regions has been highlighted by several regional studies. For example, it was found that there was a negative relationship between SM and the summer monthly Tmax in Europe (Brabson et al., 2005; Hirschi et al., 2011; Whan et al., 2015). With an increasing number of extreme temperature events, it is worthwhile to identify the driving mechanisms behind changes in annual Tmax and Tmin to improve prediction accuracy. Thus, the responses of annual Tmax and Tmin to solar activity, large-scale atmospheric circulation patterns, and SM were fully explored in this study. In contrast to previous studies, a new method called the cross wavelet analysis was adopted to reveal linkages in both time and frequency domains, rather than simply calculating their correlation coefficients.

The impacts of annual Tmax and Tmin on agriculture are also key concerns because temperature plays an important role in vegetation growth and development. The potential for annual Tmax and Tmin changes most likely influence vegetation productivity (Hatfield and Prueger, 2015). Therefore, it is necessary to explore the response of vegetation to the changing annual Tmax and Tmin which would help to develop adaptation strategies under varying environments. Moreover, increasing temperature tends to speed up the hydrological cycles, which, in turn, would lead to changes in precipitation. Theoretical models show that extreme precipitation intensity could exponentially increase with rising temperatures (Allan and Soden, 2008; Westra et al., 2013; Herath et al., 2017) at a rate determined by the Clausius–Clapeyron relationship (Herath et al., 2017) in the absence of SM limitation (Wang et al., 2017). However, little has been done ~~was done~~ to investigate the impacts of annual Tmax and Tmin on the frequency or duration of extreme precipitation events, which is why we included it in this study.

Situated in the edge of the monsoon zone, the Wei River Basin (WRB) belonging to the largest tributary of the Yellow River Basin is a climate-varied sensitive district (Zhu et al., 2016). The Guanzhong Plain, located in the middle and south of the WRB, is a major agricultural production base in western China. Local governments try to designate the plain as a national core economic development area, which will play an important role in stimulating the economic development of the surrounding areas (Huang et al., 2015a,b,c; Zhu et al., 2016). Given the significance of food security and sustainable development, a comprehensive understanding of the changes in annual Tmax and Tmin is of important significance in the WRB. Additionally, as a

typical arid and semi-arid region in China, the investigation of annual Tmax and Tmin in the WRB could provide a meaningful reference for climate change studies in other semi-arid and arid basins. Therefore, the WRB was selected as the study area for this research.

The main objectives of this study are: (1) to examine the changing patterns of annual Tmax and Tmin; (2) to fully explore the possible causes of annual Tmax and Tmin variations from the perspective of solar activity, large-scale atmospheric circulation patterns, and SM; and (3) to investigate the related implications of the changing annual Tmax and Tmin on vegetation and extreme precipitation using the cross wavelet analysis.

2. Study area and data

2.1. Study area

The WRB (Fig. 1) is located between 103.5° E–110.5° E and 33.5° N–37.5° N, and it is a major river in west-central China's Gansu and Shaanxi provinces. It originates along the north side of Niaoshu Mountain and flows from west to east through the Gansu, Ningxia and Shaanxi provinces, with a length of 818 km and drained areas of 13.5×10^4 km^2. The Jing River Basin (JRB) is the largest tributary of the WRB with drainage areas of 4.5×10^4 km^2. The Loess Plateau sits in the north of the WRB, and the Qinling Mountains sit in the south. Situated in a typical monsoon climate zone, the region is characterized by pronounced seasonality with rich precipitation and high temperatures in summer, and scarce precipitation and low temperatures in winter (Huang et al., 2014a,b; Huang et al., 2015a; Zhu et al., 2016). The main rainy season begins in June and ends in September, accounting for approximately 60% of the annual precipitation (nearly 600 mm; Zhu et al., 2016; Liu et al., 2017). The average annual temperature in the WRB ranges from 7.8 °C to 13.5 °C. The average summer temperature varies from 23 °C to 26 °C, and average winter temperatures range from −1 °C to −3 °C (Huang et al., 2014a,b).

2.2. Data

Daily precipitation data and the Tmax and Tmin from 21 National Meteorological Observatory stations were obtained from the National Climate Center of the China Meteorological Administration, covering the period from January 1st, 1958 to December 31st, 2008. The annual Tmax and Tmin dataset was obtained based on the annual maximum and minimum sampling method. The weather stations used in the study provided reasonable spatial coverage and include a variety of topographic features and climatic regions in the WRB (Fig. 1 and Table 1). Note that among the 21 weather station, the stations Lintao, Yanan, Minxian, Foping, Zhenan and Shangzhou, which are outside but nearest to the edges of the WRB, were also chosen to reflect the change characteristics of annual Tmax and Tmin around the marginal area of the basin. The Thiessen polygon method assigns weight at each gauge station in proportion to the catchment area that is closest to that gauge. Thus, it was used to compute the annual temperature data of the WRB and two sub-basins, in which the impact of the blocking of mountains could be neglected (Bayraktar et al., 2005). Additionally, most previous studies (Zuo et al., 2014; Huang et al., 2014a,b,c; Jiang et al., 2015; Zhu et al., 2016) on hydro-meteorological variations of the WRB are also based on the data at the 21 stations.

There are also three hydrological stations in the river, which are the control sites of the Upstream, the JRB, and the WRB. Thus, the river was divided into two sub-regions including the Upstream and the JRB (for the related stations included in each sub-region, see Table 2) to fully reflect the regional features of the annual Tmax and Tmin variability in the WRB.

To explore the possible causes of the changing annual Tmax and Tmin in the basin from the perspective of solar activity, large-scale atmospheric circulation patterns and SM, the correlations among annual Tmax, Tmin and the total sunspots number (SSN), Arctic Oscillation (AO), Pacific Decadal Oscillation indices (PDOI), and SM were investigated. Yearly SSN is used as a proxy of solar activity and can be downloaded freely from http://sidc.oma.be/silso/datafiles. Monthly PDOI is defined as the leading principal component of the North Pacific monthly sea surface temperature variability, which is closely related to the variability of annual Tmax and Tmin (Jakob and Walland, 2016; Zhong et al., 2017). It can be downloaded from http://research.jisao.washington.edu/pdo/. The AO is an important mode of climatic change in the Northern Hemisphere and is closely related to climate variations in middle- and high-latitude regions (e.g. Toreti et al., 2010); monthly AO can be downloaded from https://www.ncdc.noaa.gov/teleconnections/ao/. Moreover, the Normalized Differential Vegetation Index (NDVI) data (1982–2008) derived from the Land Processes Distributed Active Archive Center of the National Aeronautics and Space Administration (https://lpdaac.usgs.gov/) was used to explore the vegetation coverage's response to the changing patterns of annual Tmax and Tmin. In addition, the gridded yearly SM data covering 1958–2008, simulated by the Variable Infiltration Capacity model are obtained, and the gridded SM within the catchment area controlled by each hydrological station is averaged for use (Huang et al., 2017).

3. Methodology

3.1. Modified Mann-Kendall trend test method

The original Mann-Kendall (MK) trend test is a non-parametric method for the assessment of monotonic trends in time series (Mann, 1945; Kendall, 1955; Hamed and Rao, 1998). It has been widely used and recommended by the World Meteorological Organization. However, the results of a MK test would be affected by the autocorrelation in hydro-meteorological time series. Hence, the modified Mann-Kendall (MMK) trend test (Mann, 1945; Kendall, 1955; Hamed and Rao, 1998) was employed to estimate the trends of annual Tmax, Tmin and NDVI series in the WRB. The MMK trend test has been proven to be robust in capturing the trends in the hydro-meteorological time series. Details about MMK can be found in Huang et al. (2014c). The significant trend obtained by the MMK test was assessed at the 95% confidence level.

3.2. The Cloud model

The Cloud model proposed by Li et al. (1998) is an uncertainty technology that could provide an effective tool to quantitatively estimate qualitative analysis (Li et al., 2009; Huang et al., 2015a; Zhu et al., 2016). Several Cloud models are defined with a normal distribution, and they are most widely used in data mining, image processing, uncertainty reasoning, etc. (Li et al., 1998; Yang and Chen, 2007; Wang and Deng, 2007). The normal Cloud model consists of three primary numerical characteristics: Expectation (*Ex*), Entropy (*En*), and Hyper-Entropy (*He*), in order to characterize an uncertain concept (Fig. 2).

In Fig. 2, the *x*-axis denotes the range of a given hydrological or meteorological factor, reflecting the randomness of a natural phenomenon (in this study, annual Tmax or Tmin series), while the *y*-axis represents the degree of certainty of the given factor. Basically, the degree of certainty is the membership degree in fuzzy set theory that reflects the fuzziness of a natural phenomenon. As Fig. 2 shows, *Ex*, in the center, is the mean of annual Tmax or Tmin series. *En*, denoted by the length of the horizontal arrow, is used to describe the dispersion of annual Tmax or Tmin series, which is the uncertainty of annual Tmax or Tmin series. This parameter reflects the fuzziness and uniformity of annual Tmax or Tmin series. A smaller *En* means a more uniform of annual Tmax or Tmin series. With regard to the *He*, it is the entropy of the *En*. *He* is used to describe the randomness and stability of annual Tmax or Tmin series which is denoted by the thickness of the cloud with the given annual Tmax or Tmin value. Similarly, a smaller *He* indicates a more stable annual Tmax or Tmin series. More details about the

Table 1
The information of weather stations in the WRB.

No.	Weather station	Latitude (N)	Longitude (E)	Altitude (m)	Tmax (°C)	Tmin (°C)
1	Baoji	34.35	107.13	612	41.60	−9.44
2	Changwu	35.20	107.80	1206	37.60	−18.34
3	Foping	33.52	107.98	827	38.70	−9.15
4	Guyuan	36.00	106.27	1753	34.60	−22.70
5	Huajialing	35.38	105.00	2450	28.40	−20.28
6	Huanxian	36.58	107.30	1255	38.60	−20.15
7	Huashan	34.48	110.08	2064	29.00	−19.38
8	Lintao	35.35	103.85	1893	36.10	−20.25
9	Luochuan	35.82	109.50	1159	37.50	−18.07
10	Minxian	34.43	104.02	2315	33.30	−20.25
11	Pingliang	35.55	106.67	1346	36.00	−16.79
12	Shangzhou	33.87	109.97	742	40.70	−10.10
13	Tianshui	34.58	105.75	1141	38.20	−12.43
14	Tongchuan	35.08	109.07	978	37.70	−14.42
15	Wugong	34.25	108.22	447	42.00	−10.69
16	Wuqi	36.92	108.17	1331	38.30	−22.14
17	Xian	34.30	108.93	397	41.80	−9.95
18	Xifengzhen	35.73	107.63	1421	36.40	−16.84
19	Xiji	35.97	105.72	1916	33.40	−23.23
20	Yanan	36.60	109.50	958	39.30	−18.94
21	Zhenan	33.43	109.15	693	40.20	−8.65

Note: Tmax (Tmin) in this table is the maximum (minimum) value of annual Tmax (Tmin) series (1958–2008).

Table 2
The related stations included in the Upstream and the JRB.

The sub-region	Stations
The Upstream	Baoji
	Guyuan
	Huajialing
	Lintao
	Minxian
	Tianshui
	Xiji
The JRB	Changwu
	Guyuan
	Huanxian
	Pingliang
	Wugong
	Wuqi
	Xian
	Xifengzhen

Table 3
The numerical characteristics of temperature extremes cloud of the Upstream, the JRB and the WRB.

Catchment	Tmax			Tmin		
	Ex	*En*	*He*	*Ex*	*En*	*He*
Upstream	29.71	1.23	0.46	−20.05	1.79	0.58
The JRB	32.98	1.19	0.37	−18.32	2.12	0.63
The WRB	32.45	0.96	0.37	−15.23	1.74	0.48

algorithm can be found in Li et al. (1998, 2009) and Huang et al. (2015a). In this present study, the Thiessen polygon method was used to compute the annual Tmax and Tmin data of the WRB and two sub-basins from the 15 stations (see Table 2) and the other 6 related stations. Finally, the annual Tmax and Tmin data in 1958–2008 in the WRB and two sub-basins were used as input for the Cloud model to

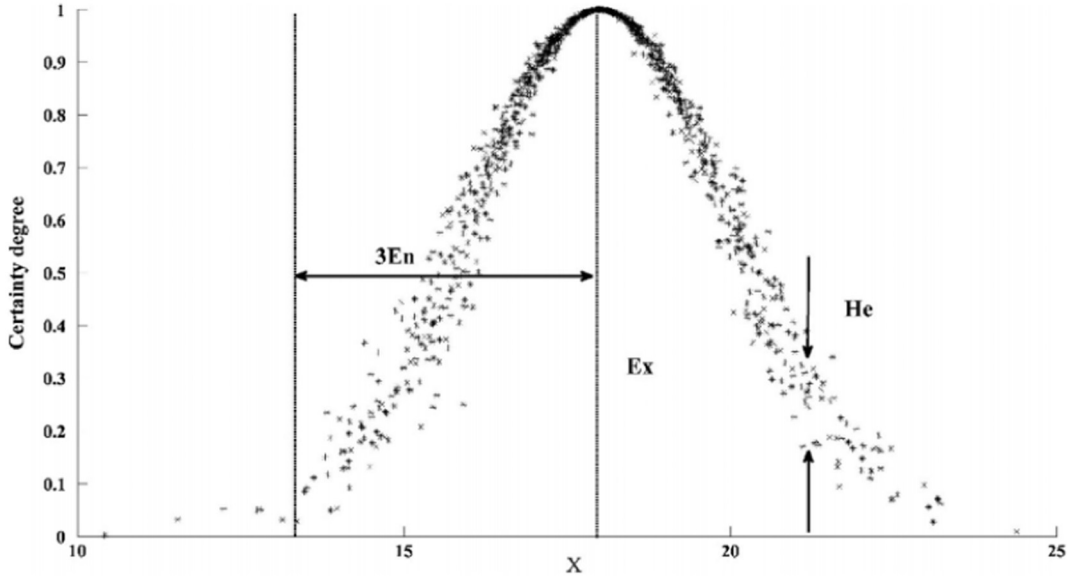

Fig. 2. The three numerical characteristics of the Cloud model. *X* denotes the input data for the Cloud model; *Ex*, *En*, and *He* represent the three numerical characteristics of the Cloud model.

obtain the three numerical characteristics: Expectation (*Ex*), Entropy (*En*), and Hyper-Entropy (*He*) of annual Tmax and Tmin series, which were shown in Table 3.

3.3. The cross wavelet analysis

The cross wavelet analysis is a new technique that combines a wavelet transform with cross spectrum analysis. Therefore, it is appropriate to assess the change characteristics and coupled oscillations of two time series in both the time and frequency domains (Hudgins et al., 1993; Torrence and Compo, 1998; Huang et al., 2015a,b,c). For two given time series x_n and y_n, their cross wavelet transform can be defined as $W^{XY} = W^X W^{Y*}$, where * is their complex conjugation. The cross wavelet power is expressed as $|W^{XY}|$. The complex argument arg (W^{xy}) can be regarded as the local relative phase of these two time series in the time-frequency field. The theoretical distribution of the cross wavelet power between x_n and y_n with their background power spectra P_k^X and P_k^Y (Torrence and Compo, 1998) can be defined as follows:

$$D\left(\frac{W_n^X(s)W_n^{Y*}(s)}{\sigma_X\sigma_Y} < p\right) = \frac{Z_v(p)}{v}\sqrt{P_k^X P_k^Y} \quad (1)$$

where Z_v(p) is the confidence level associated with the probability p for a probability distribution function defined by the square root of the two χ^2 distributions (Grinsted et al., 2004). The relevant codes can be downloaded from http://noc.ac.uk/using-science/crosswavelet-wavelet-coherence.

4. Results

4.1. Change patterns of annual Tmax and Tmin in the WRB

4.1.1. Temporal change patterns of annual Tmax and Tmin

The MMK trend test was used to detect the trends of annual Tmax and Tmin series in the WRB, and the results are shown in Fig. 3. Generally, the WRB is dominated by widespread increases in annual Tmax and Tmin with more than 85% of stations exhibiting positive MMK statistics or significant increasing trends at the 95% confidence level (Fig. 3). Significant increasing trends (8 out of 21 stations) in annual Tmax are mainly found in the Upstream, the JRB and the Guanzhong Plain. By contrast, the negative MMK statistics of annual Tmax recorded at three stations are geographically concentrated in the northern and eastern portions of basin (Fig. 3A). For annual Tmin, significant increasing trends at the 95% confidence level are recorded at 10 stations, mainly situated in the Upstream and the Guanzhong Plain, while three stations exhibit negative MMK statistics, with one station in the middle of the WRB indicating significant decreasing trends at the 95% confidence level (Fig. 3B). In addition, the MMK tests for the annual Tmax and Tmin series in the Upstream, the JRB, and the WRB were also conducted. It was found that the two sub-basins and the WRB are characterized by increasing annual Tmax and Tmin. The MMK statistics of the annual Tmax in the two sub-basins and the WRB are 1.27, 2.40, and 0.89, respectively, and those of annual Tmin are 2.13, 0.65, and 3.01, respectively. Overall, the increasing trend of annual Tmin is larger than that of annual Tmax. In general, these observations are consistent with the findings of previous publications (Zhou and Ren, 2011; Dashkhuu et al., 2014; Yu and Li, 2015; Jiang et al., 2016; Zhang et al., 2017).

According to the Cloud model procedures, the normal cloud computation was carried out based on the annual Tmax and Tmin time series in the two sub-basins and the WRB, and their corresponding numerical characteristics and clouds were presented in Table 3 and Fig. 4. Since *Ex* denotes the averages of annual Tmax and Tmin series, it can be observed in Table 3 and Fig. 4 that the maximum averages of annual Tmax and Tmin are found in the JRB and the WRB, respectively, while the minimum averages of annual Tmax and Tmin are all found in the Upstream. Note that *En* is defined to measure the dispersion degree and non-uniformity of the annual Tmax and Tmin time series relative to their averages. The larger the *En* value, the higher the dispersion degree and non-uniformity. Since the *En* values of annual Tmin are larger than those of annual Tmax (Table 3 and Fig. 4), it can be concluded that annual Tmin has a higher dispersion degree and is less uniform than annual Tmax both in the two sub-basins and the WRB. In order to corroborate this finding, the standard deviations of the annual Tmax and Tmin series in the Upstream, the JRB, and the WRB were calculated, which can also reflect the uniformity of annual Tmax and Tmin series. The standard deviation of the annual Tmax in the two sub-basins and the WRB are 1.31, 1.24, and 1.03, respectively, and those of the annual Tmin are 1.89, 2.22, and 1.80, respectively. The larger standard deviations indicate that annual Tmin is less uniform. It should be mentioned that *He* denotes the dispersion degree of *En* and is used to quantify the stability of the non-uniformity of the annual Tmax and Tmin. A larger *He* implies more instability. Like *En*, the *He* values of the annual Tmin are higher than those of annual Tmax, which demonstrates that annual Tmin is more unstable than annual Tmax in the entirety of WRB.

In general, annual Tmin series has a higher dispersion degree and is more non-uniform and unstable than annual Tmax series in the WRB. As the main grain-yielding area, a changeable annual Tmin is found to

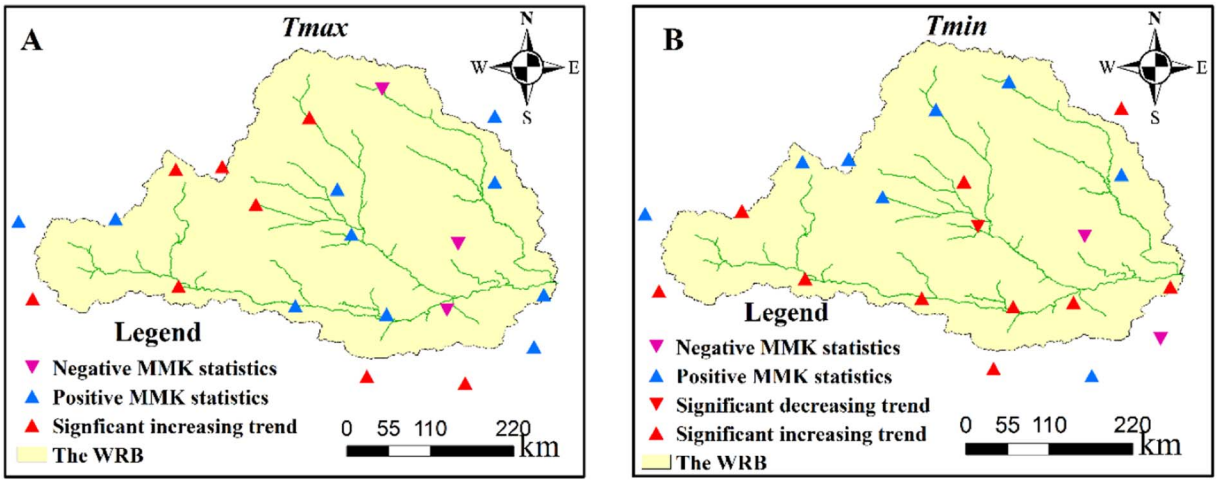

Fig. 3. MMK trend tests of Tmax and Tmin across the WRB. The blue upward triangles denote positive MMK statistics, while the purple downward triangles indicate the negative MMK statistics. The red upward/downward triangles indicate the statistically significant increasing/decreasing trend at the 95% confidence level. (For interpretation of the references to color in this figure legend, the reader is referred to the web version of this article.)

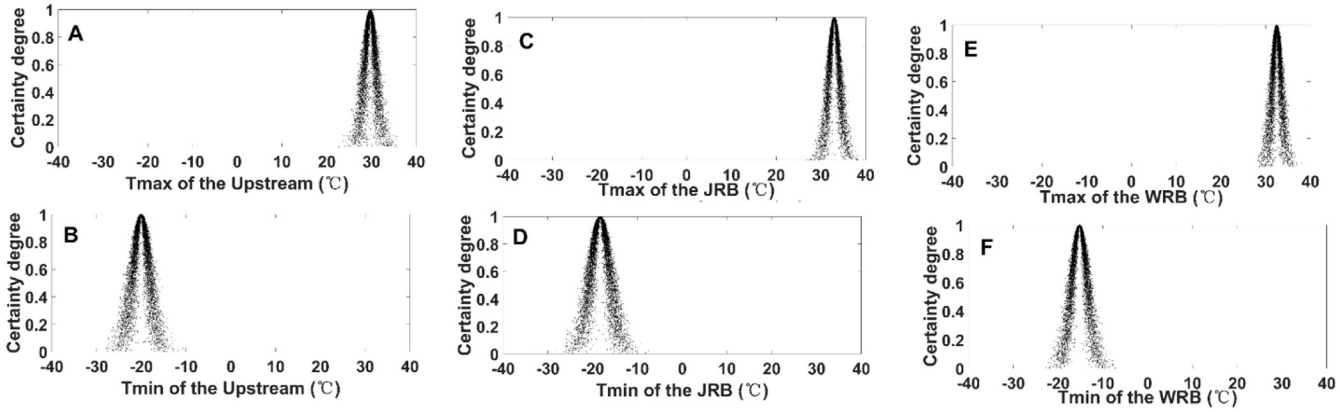

Fig. 4. The Tmax and Tmin clouds of the Upstream, the JRB and the WRB. The number of cloud drops is 10,000.

have a negative impact on food production (Hatfield and Prueger, 2015). Therefore, scientific prevention and/or adaptive strategies should be adopted by the local government.

4.1.2. Spatial change patterns of annual Tmax and Tmin

Fig. 5 shows the spatial distribution of the three numerical characteristics of the annual Tmax and Tmin clouds in the WRB. Generally, there is a strikingly irregular spatial distribution to these three numerical characteristics. The average (*Ex*) annual Tmax in the WRB ranges from 25 °C to 39.23 °C and that of annual Tmin varies from −23.23 to −9.17 °C with the lowest *Ex* found in the Upstream and the highest *Ex* found in the Guanzhong Plain (Fig. 5A and B). This may be owing to the Liupan Mountain in the Upstream, which blocks the east-west monsoon channel (Zhu et al., 2016). Besides, the capital city of Xi'an and other cities of the Shaanxi province are situated in the plain, so the higher *Ex* is may be attributed to urban heat island effects (Limsakul and Singhruck, 2016; Liu et al., 2017). Fig. 5C and D show the variation range of *En* for annual Tmin is larger than that of annual Tmax across the basin, which is consistent with the findings of Section 4.1.1. The *En* values are generally larger in the JRB and the Guanzhong Plain and lower in the northeastern portion of the WRB (Fig. 5C and D), implying that the annual Tmax and Tmin in the JRB and the plain are more uneven than other areas. This may be because the JRB is located in the Loess Plateau; and the Guanzhong Plain is near to the Qinling Mountains which mark the edge of the monsoon region. These areas are sensitive to climate change and/or the abnormalities of the monsoon (Huang et al., 2014b; Zhu et al., 2016). Thus, the annual Tmax and Tmin in these areas exhibit clear variations. Similarly, the *He* values of the annual Tmax and Tmin in the WRB have striking differences. Fig. 5E shows that the higher *He* values of annual Tmax are mainly found in the Loess Plateau (in the upper reaches of the JRB), suggesting that the stability of annual Tmax in this district is less than that of other regions of the basin. By contrast, higher *He* values of annual Tmin are mostly focused in the downstream area of the JRB and the Guanzhong Plain, implying annual Tmin is less stable in these areas. This may be due to their locations and intensifying human activities in the region (Zhou and Ren, 2011; Huang et al., 2014b). Overall, the spatial change patterns of annual Tmax and Tmin, based on the three numerical characteristics of the normal Cloud model, indicate that annual Tmax and Tmin in the JRB, which belongs to the Loess Plateau, have higher dispersion degrees and are less uniform and stable compared with other regions of the WRB.

4.2. Causes of annual Tmax and Tmin variations in the WRB

Apart from anthropogenic factor, some other factors may also influence the variations of annual Tmax and Tmin. In order to explore the potential causes of changing annual Tmax and Tmin from the perspective of solar activity, large-scale atmospheric circulation patterns, and SM, the correlations among annual Tmax and Tmin time series in the WRB and SSN, AO, PDOI and SM series based on the cross wavelet analysis were investigated (Figs. 6–8).

4.2.1. Teleconnection among annual Tmax, Tmin, and SSN

Fig. 6 displays the cross wavelet transforms of SSN and annual Tmax and Tmin in the Upstream, the JRB, and the WRB. Obviously, SSN exerts a strong influence on the variations of annual Tmax and Tmin across the WRB. Specifically, Fig. 6A shows that SSN has a statistically significant negative correlation with the annual Tmax series in the Upstream, with a 9–12 year signal in 1970–1990 at the 95% confidence level. SSN also shows a statistically significant negative correlation with annual Tmax series in the Upstream with a 8–14 year signal in 1992–2008. Fig. 6B illustrates that SSN and annual Tmin have a statistically significant negative correlation in the Upstream with a signal of 7–14 year from 1975 to 2007.

For the JRB, Fig. 6C shows SSN has a statistically significant negative correlation with annual Tmax variations in the JRB with a 9–12 years signal from 1976 to 2006 at the 95% confidence level. Fig. 6D indicates SSN has statistically significant negative correlations with annual Tmin in the JRB with a 9–10 years signal in 1963–1970, a 9–12 year signal in 1986–2006 and a 7–9 year signal in 1986–1998 at the 95% confidence level. Besides, SSN also has a statistically positive correlation with annual Tmin in the JRB with a 7–9 year signal in 1976–1984 at the 95% confidence level (Fig. 6D).

For the WRB, there is a statistically significant negative correlation between SSN and annual Tmax, with a signal of 8–12 years from 1975 to 2007 (Fig. 6E). In addition, SSN exhibits statistically significant negative correlations with annual Tmin in the WRB with a 9–10 year signal from 1963 to 1983 and a 7–14 year signal from 1987 to 2006, and it exhibits a positive correlation with a 7–9 year signal from 1980 to 1982 at the 95% confidence level. In general, these significant correlations among SSN, annual Tmax, and annual Tmin in the Upstream, the JRB, and the WRB suggest that solar activity has a remarkable impact on the variations of the annual Tmax and Tmin series.

4.2.2. Teleconnection among AO, PDOI, annual Tmax, and annual Tmin

The cross wavelet transforms between AO, PDOI, annual Tmax, and annual Tmin in the WRB are displayed in Fig. 7. Fig. 7A demonstrates that the AO has a statistically significant negative correlation with annual Tmax in the WRB, with a 1–5 year signal from 1964 to 1970 at the 95% confidence level. Additionally, AO exhibits a statistically significant negative correlation with annual Tmin at the 95% confidence level with a 7–9 year signal from 1983 to 1994 (Fig. 7B). As shown in Fig. 7C, there are statistically significant negative correlations between annual Tmax and PDOI, with a 2–4 year signal in 1993–2000 and a 5 year signal around 1988. Fig. 7D illustrates that the PDOI has

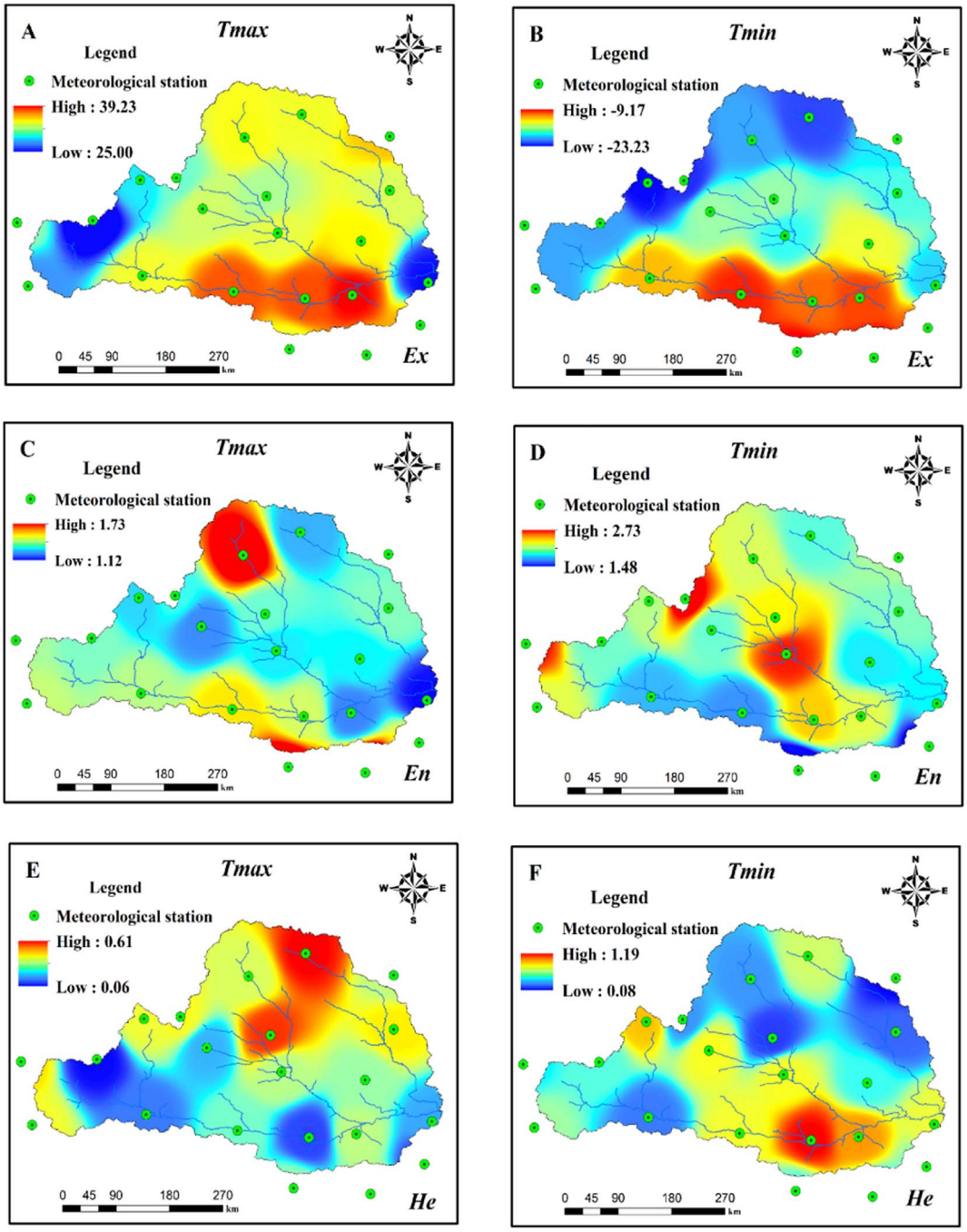

Fig. 5. Spatial distribution of the three numerical characteristics of Tmax and Tmin in the WRB. On the left are the *Ex* (A), *En* (C), and *He* (E) of Tmax, while the right are the *Ex* (B), *En* (D), and *He* (F) of Tmin.

statistically significant negative correlations with annual Tmin variations in the WRB with a 3–4 year signal in 1983–1988 and a 5–6 year signal in 1996–2000 at the 95% confidence level. In addition, the PDOI shows statistically significant positive correlations with annual Tmin in the WRB with a 1–3 year signal from 1990 to 1996, and a 8–9 year signal from 1990 to 1998 at the 95% confidence level. Similar correlations among AO, PDOI, annual Tmax, and annual Tmin in the Upstream and the JRB have also been observed (for brevity, results are not shown). These significant correlations among annual Tmax, annual Tmin, AO, and PDOI series demonstrate that large-scale atmospheric circulation patterns play important roles in the variations of annual Tmax and Tmin in the WRB.

4.2.3. Connections among SM, annual Tmax, and annual Tmin

Fig. 8 exhibits the cross wavelet transforms between SM, annual Tmax, and annual Tmin in the WRB. Fig. 8A shows that there is a statistically significant negative correlation between the SM and annual Tmax variations at the 95% confidence level, with a 2–5 year signal from 1963 to 1970 and a 6 year signal from 1963 to 1968. Fig. 8B indicates that SM also has statistically significant negative correlations with annual Tmin variations in the WRB at the 95% confidence level, with a 7–8 year signal from 1978 to 1990 and a 4–5 year signal from 1984 to 1986. Similar relations among SM, annual Tmax, and annual Tmin in the two sub-basins have also been found (for brevity, results are not shown). These findings suggest that changes of annual Tmax and Tmin in the WRB are also significantly linked to SM.

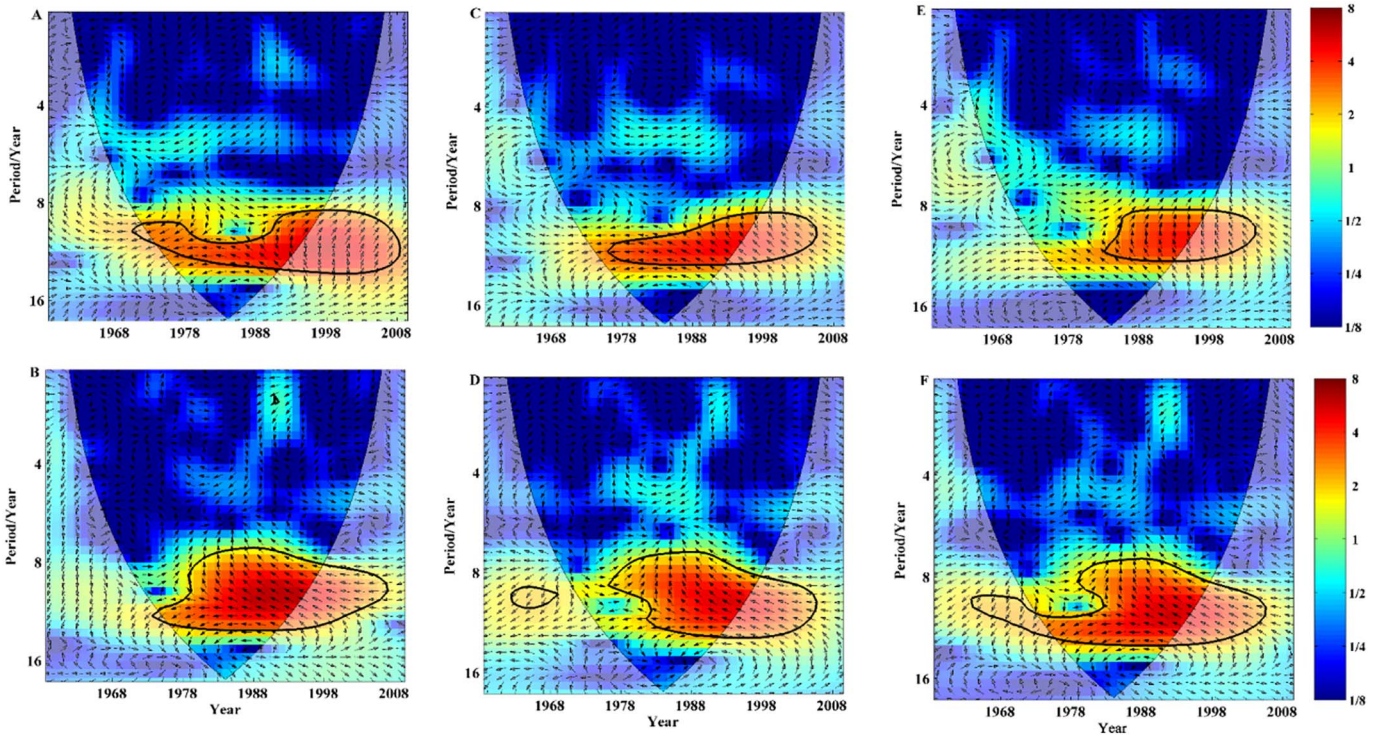

Fig. 6. The cross wavelet transforms between the SSN and Tmax and Tmin series in the Upstream (A and B), the JRB (C and D) and the WRB (E and F). On the top is those of the Tmax series, while on the bottom is those of the Tmin series. The 95% significance confidence level against red noise is exhibited as a thick contour, and the relative phase relationship is denoted as arrows (with anti-phase pointing left, in-phase pointing right). The color bar on the right denotes wavelet energy. (For interpretation of the references to color in this figure legend, the reader is referred to the web version of this article.)

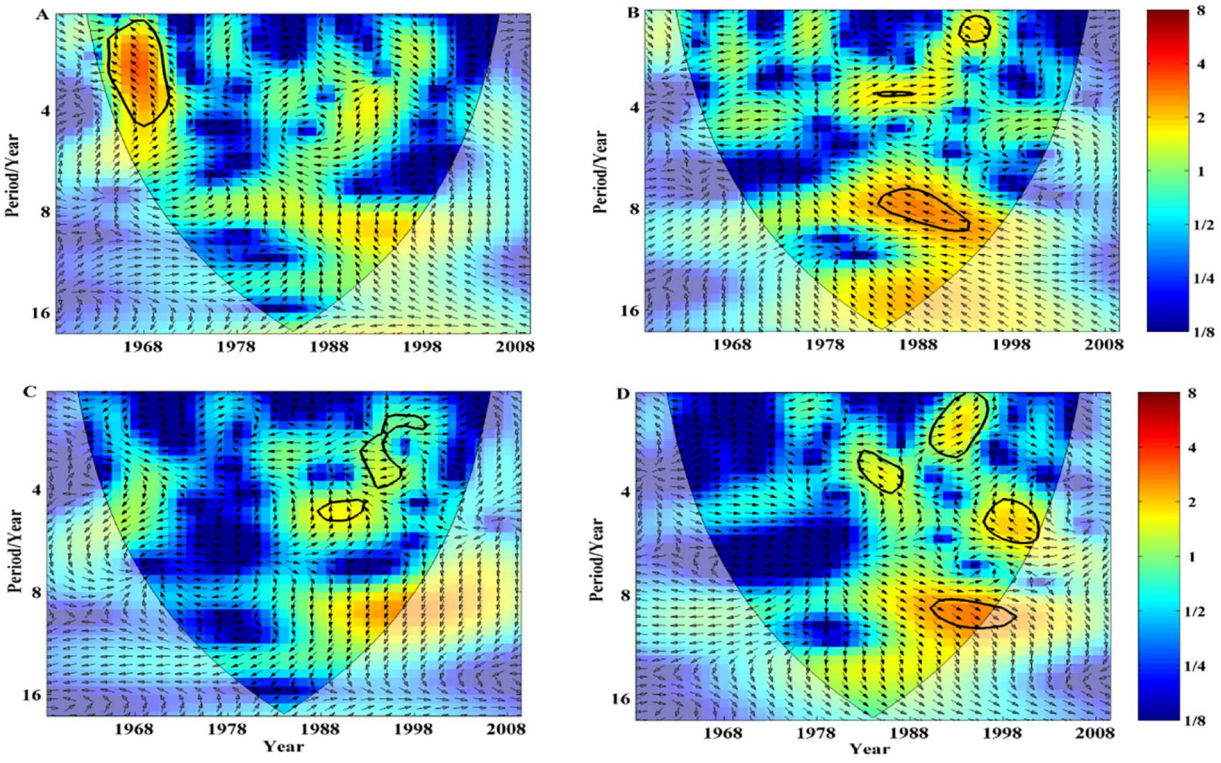

Fig. 7. The cross wavelet transforms among the AO (A and B), PDO (C and D) and Tmax and Tmin series in the WRB. On the left is that of the Tmax series, while on the right is that of the Tmin series.

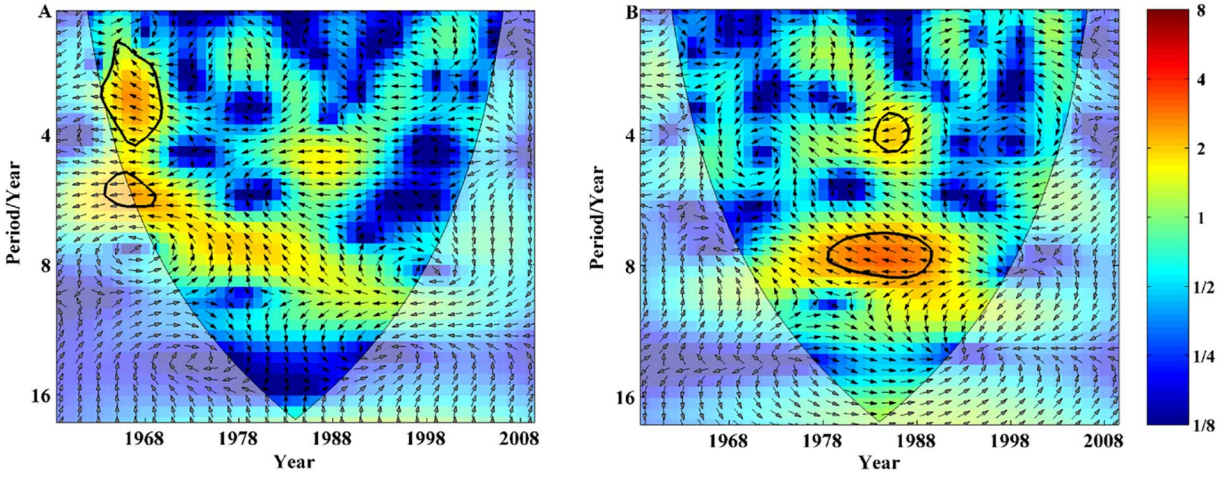

Fig. 8. The cross wavelet transforms between SM and Tmax and Tmin series in the WRB: (A) Tmax and (B) Tmin.

4.3. Implications of changing annual Tmax and Tmin in the WRB

4.3.1. Effects of changing annual Tmax and Tmin on NDVI

Temperature plays an important role in the growth and development of vegetation and would also affect the pollination of plants (Hatfield and Prueger, 2015). Since the Guanzhong Plain in the middle and south of the WRB is a highly important agricultural production base, it is necessary to investigate the effects of changing annual Tmax and Tmin on NDVI, which would provide scientific insight for local agricultural production.

Similar to annual Tmax and Tmin in the WRB, there is a significant increasing trend in vegetation coverage at the 95% confidence level with MMK statistic of 3.59. Fig. 9 shows the cross wavelet transforms between the NDVI and annual Tmax and Tmin series spanning 1982–2008 in the WRB. It is illustrated that annual Tmax has statistically significant positive correlations with the NDVI series, with a signal of 3–5 years in 1988–1993 and a 1–2 year signal in 1996–1999 (Fig. 9A). Fig. 9B indicates there is a statistically significant positive correlation between the annual Tmin and NDVI series with a signal of 8–9 years from 1988 to 1996. These significant correlations imply that increasing annual Tmax and Tmin values have exerted remarkable influence on the rapidly increasing vegetation coverage, which suggests that the local government should consider their potential consequences (e.g. major vegetation shifts, Bokhorst et al., 2012).

4.3.2. Effects of changing annual Tmax and Tmin on precipitation extremes

Liu et al. (2017) claimed that the stationarity of precipitation extremes in the Upstream of the WRB is invalid, based in part on notable changes in the late 1960s. Therefore, we decided to explore the detailed linkages between increasing annual Tmax and Tmin and precipitation extremes in the Upstream, which would help us to better understand precipitation extreme variations for improved weather predictions and water resources management.

The annual maximum 1-day precipitation (RX1day), the frequency of extremely wet day precipitation (R95D), and consecutive wet days (CWD) were selected as the intensity, frequency, and duration indices of precipitation extremes, respectively (Limsakul and Singhruck, 2016; Liu et al., 2017). Fig. 10 shows the cross wavelet transforms between annual Tmax and Tmin and precipitation extremes in the Upstream. Fig. 10A demonstrates that the annual Tmax has a statistically significant positive correlation with the RX1day variations at the 95% confidence level, with a 2–4 year signal from 1967 to 1972. There is a statistically significant negative correlation between annual Tmin and RX1day series, with a signal of 15–17 year from 1979 to 1994 (Fig. 10B). For the frequency index, annual Tmax shows a statistically significant negative correlation with the R95D with a 2–4 year signal in 1965–1971 (Fig. 10C). By comparison, annual Tmin has a statistically significant negative correlation with R95D with a 1-year signal in 1991–1992 (Fig. 10D). For the duration index, annual Tmax exhibits a statistically significant negative correlation with the CWD with a

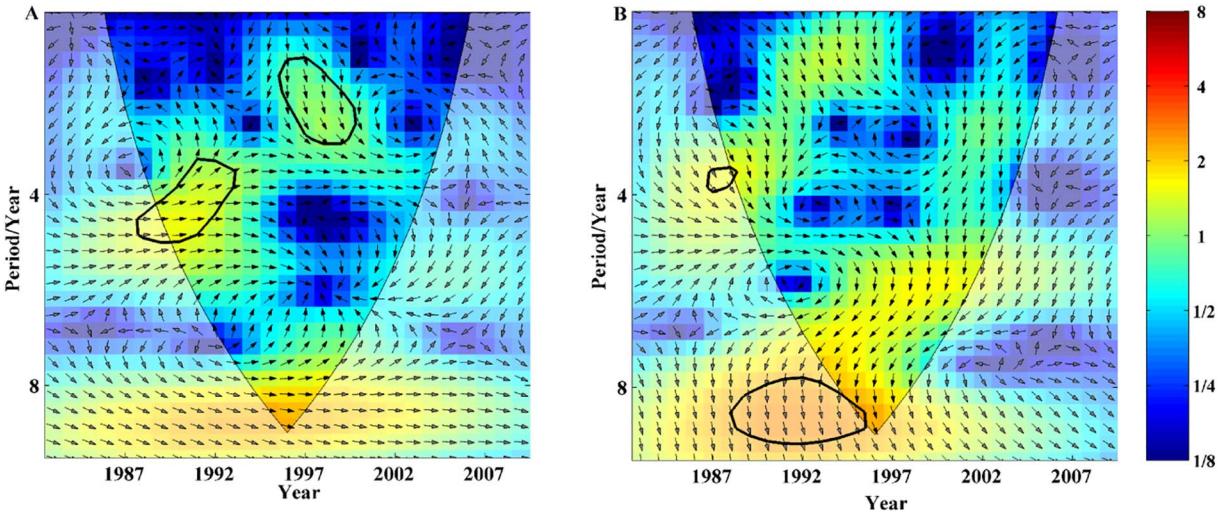

Fig. 9. The cross wavelet transforms between NDVI and Tmax and Tmin series spanning 1982–2008 in the WRB: (A) Tmax and (B) Tmin.

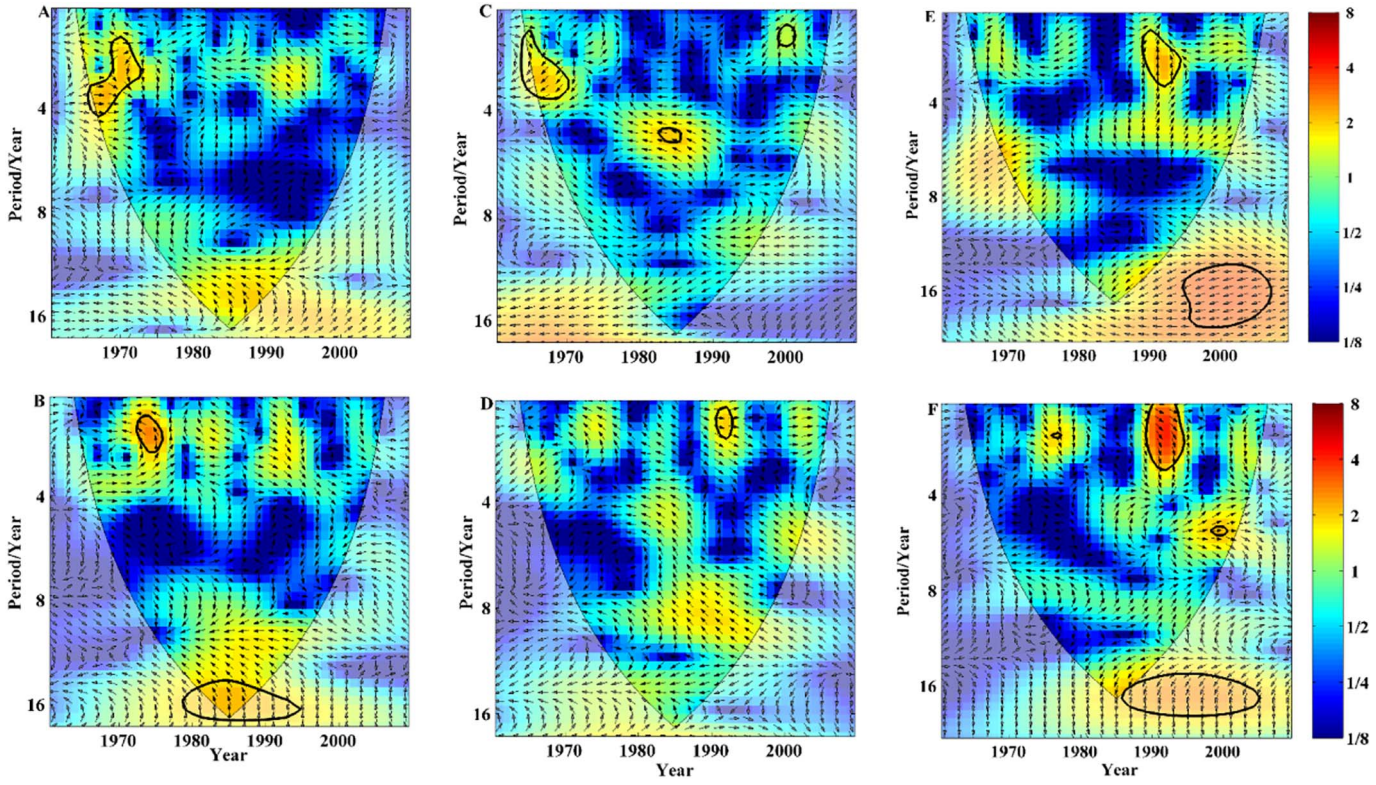

Fig. 10. The cross wavelet transforms between Tmax and Tmin and precipitation extremes intensity (A and B), frequency (C and D) and duration (E and F) in the Upstream of the WRB. On the top is those of the Tmax series, while on the bottom is those of the Tmin series.

2–3 year signal in 1989–1993 and a 15–17 year signal in 1996–2008 (Fig. 10E). There is also a statistically significant positive correlation between the annual Tmin in the Upstream and the CWD with a 1–3 year signal from 1989 to 1995, and there is a statistically significant negative correlation in 1987–2006, with a signal of 15–16 year (Fig. 10F). A comparison of Fig. 10 shows that CWD and RX1day are most strongly influenced by the changing annual Tmax and Tmin.

5. Discussion

The relationships between SSN and annual Tmax and Tmin are the strongest (Figs. 6–8), which indicates that the variations of the annual Tmax and Tmin in the WRB are more strongly influenced by solar activity than other factors mentioned above. Since solar radiation is the source of energy (Valev, 2006) it could modulate large-scale atmospheric circulation patterns variations through geomagnetic activity (Valev, 2006; Qian, 2017).

Although the relationships between SSN and annual Tmax and Tmin are strongest, there remain differences in the time and frequency domains in different regions, which may explain the different spatial change patterns in the annual Tmax and Tmin in the Upstream, the JRB, and the WRB (see Section 4.1.2).

The relationships among annual Tmin, SSN, AO, PDOI, and SM are generally stronger than those among the same factors and annual Tmax, indicating that annual Tmin is more sensitive to those factors' influences. Further, it could also explain the larger increases, higher dispersion degree, greater non-uniformity, and larger instability in the annual Tmin than annual Tmax in the WRB (see Section 4.1.1).

When there are time overlaps in different indices showing correlations with annual Tmax and Tmin in the WRB, they usually have different frequencies. For instance, both SSN and PDO have statistically significant correlations with the annual Tmax series in the WRB in 1993–2000, but with different frequency signals.

These findings demonstrate that the variations of the annual Tmax and Tmin in the WRB are closely linked to the combined influences of solar activity, large-scale atmospheric circulation patterns, and SM However, whether the interactions among these indices are reinforcing or offsetting each other requires further investigation in future studies.

The correlations among annual Tmax, Tmin, the RX1day, R95D, and CWD imply that increasing annual Tmax and Tmin values are closely related to precipitation extremes in terms of the duration, intensity and frequency in the WRB. In addition, the change point of the R95D in 1969 (Liu et al., 2017) corresponds to the period in which annual Tmax is statistically negatively correlated with the R95D in 1965–1971, which suggests that the increasing annual Tmax might be one of the potential causes of the nonstationary extreme precipitation series in the Upstream of the WRB.

6. Conclusions

The investigation of annual Tmax and Tmin is important to better understand the regional response of temperatures to changing environments. In this study, a comprehensive investigation of the spatial-temporal change patterns, potential causes and relevant implications of temperature extremes in the WRB was performed based on the Cloud model and cross wavelet analysis.

Generally, the WRB is characterized by increasing annual Tmax and Tmin values, although the increasing trend in annual Tmin is larger than that of annual Tmax. In addition, annual Tmin has a higher dispersion degree and is less uniform and stable than annual Tmax. The asymmetric variations of annual Tmax and Tmin can be explained by the stronger influences of solar activity, large-scale atmospheric circulation patterns, and SM on annual Tmin than on annual Tmax.

Topography plays an important role in affecting the spatial variations of the three numerical characteristics of the annual Tmax and Tmin clouds in the WRB. Specifically, the lowest *Ex* was found in the Upstream and the highest *Ex* was found in the Guanzhong Plain owing to the Liupan Mountain in the Upstream and the urban heat island

effect in the plain. The *En* and *He* values were larger in the JRB (the Loess Plateau), implying that annual Tmax and Tmin in this region are more uneven and instable than other regions in the WRB. These findings can also be attributed to the differences in the relationships between solar activity and annual Tmax and Tmin in the time and frequency domains in different regions.

Additionally, the correlations between the changing annual Tmax and Tmin and NDVI suggest that the increasing annual Tmax and Tmin have exerted remarkable implications on the rapidly increasing vegetation coverage in the WRB. Their similar relationships with precipitation extremes also suggest that variations in annual Tmax and Tmin will impact the duration, intensity, and frequency of precipitation extremes in the WRB. Also, the increasing annual Tmax might also be one of a potential cause of the nonstationary extreme precipitation series in the Upstream of the WRB.

In conclusion, the Cloud model provides a new approach and quantitative measure for estimating the uniformity and stability of temperature extremes. Besides, our findings suggest that solar activity, large-scale atmospheric circulation patterns, and SM have the potential to improve the prediction of annual Tmax and Tmin in the study region. Moreover, the findings of this study may facilitate more informed decision-makings in terms of both the scientific mitigation of disasters and efficient water resources management.

Acknowledgement

This research was supported by the National Natural Science Foundation of China (51709221), Planning Project of Science and Technology of Water Resources of Shaanxi (2017slkj-19), National Natural Fund Major Research Plan (91325201), the National Department Public Benefit Research Foundation of Ministry of Water Resources (201501058), and Project of School of Water Resources and Hydropower of Xi'an University of Technology (2016ZZKT-15).

References

Allan, R.P., Soden, B.J., 2008. Atmospheric warming and the amplification of precipitation extremes. Science 321 (5895), 1481–1484.
Bayraktar, H., Turalioglu, F.S., Şen, Z., 2005. The estimation of average areal rainfall by percentage weighting polygon method in Southeastern Anatolia Region, Turkey. Atmos. Res. 73 (1–2), 149–160.
Bokhorst, S., Tømmervik, H., Callaghan, T.V., et al., 2012. Vegetation recovery following extreme winter warming events in the sub-Arctic estimated using NDVI from remote sensing and handheld passive proximal sensors. Environ. Exp. Bot. 81 (3), 18–25.
Brabson, B.B., Lister, D.H., Jones, P.D., et al., 2005. Soil moisture and predicted spells of extreme temperatures in Britain. J. Geophys. Res. Atmos. 110 (5), 755–765.
Dashkhuu, D., Kim, J.P., Chun, J.A., et al., 2014. Long-term trends in daily temperature extremes over Mongolia. Weather Clim. Extrem. 56, 26–33.
Donat, M.G., Alexander, L.V., 2012. The shifting probability distribution of global daytime and night-time temperatures. Geophys. Res. Lett. 39 (14), 132–151.
Fonseca, D., Carvalho, M.J., Marta-Almeida, M., et al., 2015. Recent trends of extreme temperature indices for the Iberian Peninsula. Phys. Chem. Earth A/B/C 94, 66–76.
Grinsted, A., Moore, J.C., Jevrejeva, S., 2004. Application of the cross wavelet transform and wavelet coherence to geophysical time series. Nonlinear Proc. Geoph. 11, 561–566.
Hamed, K.H., Rao, A.R., 1998. A modified Mann–Kendall trend test for autocorrelated data. J. Hydrol. 204, 182–196.
Hatfield, J.L., Prueger, J.H., 2015. Temperature extremes: effect on plant growth and development. Weather Clim. Extrem. 10, 4–10.
Herath, S.M., Sarukkalige, R., Nguyen, V.T.V., 2017. Evaluation of empirical relationships between extreme rainfall and daily maximum temperature in Australia. J. Hydrol. http://dx.doi.org/10.1016/j.jhydrol.2017.01.060.
Hirschi, M., Seneviratne, S.I., Alexandrov, V., et al., 2011. Observational evidence for soil-moisture impact on hot extremes in southeastern Europe. Nat. Geosci. 4 (1), 17–21.
Huang, S., Chang, J., Huang, Q., et al., 2014a. Spatio-temporal changes and frequency analysis of drought in the Wei River Basin, China. Water Resour. Manag. 28 (10), 3095–3110.
Huang, S., Hou, B., Chang, J., et al., 2014b. Spatial-temporal change in precipitation patterns based on the cloud model across the Wei river basin, China. Theor. Appl. Climatol. 120 (1–2), 391–401.
Huang, S., Chang, J., Huang, Q., et al., 2014c. Spatio-temporal changes in potential evaporation based on entropy across the Wei river basin. Water Resour. Manag. 28 (13), 4599–4613.
Huang, S., Hou, B., Chang, J., et al., 2015a. Spatial-temporal change in precipitation patterns based on the cloud model across the Wei River Basin, China. Theor. Appl. Climatol. 120 (1), 391–401.
Huang, S., Huang, Q., Chang, J., et al., 2015b. Drought structure based on a nonparametric multivariate standardized drought index across the Yellow river basin, China. J. Hydrol. 530, 127–136.
Huang, S., Chang, J., Leng, G., et al., 2015c. Integrated index for drought assessment based on variable fuzzy set theory: a case study in the Yellow River basin, China. J. Hydrol. 527 (527), 608–618.
Huang, S., Huang, Q., Leng, G., et al., 2017. Variations in annual water-energy balance and their correlations with vegetation and soil moisture dynamics: a case study in the Wei River Basin, China. J. Hydrol. 546, 515–525.
Hudgins, L., Friehe, C.A., Mayer, M.E., 1993. Wavelet transforms and atmospheric turbulence. Phys. Rev. Lett. 71, 3279–3282.
IPCC, 2013. In: Stocker, T.F., Qin, D., Plattner, G.-K., Tignor, M., Allen, S.K., Boschung, J., Nauels, A., Xia, Y., Bex, V., Midgley, P.M.E. (Eds.), Summary for Policymakers. Climate Change 2013: The Physical Science Basis. Contribution of Working Group I to the Fifth Assessment Report of the Intergovernmental Panel on Climate Change.
Jakob, D., Walland, D., 2016. Variability and long-term change in Australian temperature and precipitation extremes. Weather Clim. Extrem. 14, 36–55.
Jiang, C., Xiong, L.H., Wang, D.B., et al., 2015. Separating the impacts of climate change and human activities on runoff using the Budyko-type equations with time-varying parameters. J. Hydrol. 522, 326–338.
Jiang, C., Mu, X., Wang, F., et al., 2016. Analysis of extreme temperature events in the Qinling Mountains and surrounding area during 1960–2012. Quat. Int. 392 (4), 155–167.
Kendall, M.G., 1955. Rank Correlation Methods. Griffin, London.
Kristoufek, L., 2016. Has global warming modified the relationship between sunspot numbers and global temperatures? Phys. A 468, 351–358.
Kruger, A.C., Sekele, S.S., 2013. Trends in extreme temperature indices in South Africa: 1962–2009. Int. J. Climatol. 33 (3), 661–676.
Leng, G., Tang, Q., Rayburg, S., 2015. Climate change impacts on meteorological, agricultural and hydrological droughts in China. Glob. Planet. Chang. 126, 23–34.
Li, D., Han, J., Shi, X., et al., 1998. Knowledge representation and discovery based on linguistic atoms. Knowl.-Based Syst. 10 (7), 431–440.
Li, D., Liu, C., Gan, W., 2009. A new cognitive model: Cloud model. Int. J. Intell. Syst. 24 (3), 357–375.
Limsakul, A., Singhruck, P., 2016. Long-term trends and variability of total and extreme precipitation in Thailand. Atmos. Res. 169, 301–317.
Liu, S., Huang, S., Huang, Q., et al., 2017. Identification of the non-stationarity of extreme precipitation events and correlations with large-scale ocean-atmospheric circulation patterns: a case study in the Wei River Basin, China. J. Hydrol. 548, 184–195.
Mann, H.B., 1945. Nonparametric tests against trend. Econometrica 13, 245–259.
Ngo, N.S., Horton, R.M., 2015. Climate change and fetal health: the impacts of exposure to extreme temperatures in New York City. Environ. Res. 144, 158–164.
Nyeko-Ogiramoi, P., Willems, P., Ngirane-Katashaya, G., 2013. Trend and variability in observed hydrometeorological extremes in the Lake Victoria basin. J. Hydrol. 489 (3), 56–73.
Orlowsky, B., Seneviratne, S.I., 2012. Global changes in extreme events: regional and seasonal dimension. Clim. Chang. 110 (3), 669–696.
Qian, Z., 2017. Evidence for the effect of sunspot activity on the El Niño/Southern Oscillation. New Astron. 52, 1–7.
Toreti, A., Xoplaki, E., Maraun, D., et al., 2010. Characterisation of extreme winter precipitation in Mediterranean coastal sites and associated anomalous atmospheric circulation patterns. Nat. Hazards Earth Syst. Sci. 10 (5), 1037–1050.
Torrence, C., Compo, G.P., 1998. A Practical Guide to Wavelet Analysis. Bull. Am. Meteorol. Soc. 79 (1), 61–78.
Trenberth, K.E., 2011. Changes in precipitation with climate change. Clim. Res. 47 (1), 123–138.
Valev, D., 2006. Statistical relationships between the surface air temperature anomalies and the solar and geomagnetic activity indices. Phys. Chem. Earth A/B/C 31 (1–3), 109–112.
Wang, H., Deng, Y., 2007. In: Spatial clustering method based on cloud model. Proceedings of IEEE 4th International Conference on Fuzzy Systems and Knowledge Discovery. vol. 2. pp. 272–276 (August 2007).
Wang, D., Hagen, S.C., Alizad, K., 2013. Climate change impact and uncertainty analysis of extreme rainfall events in the Apalachicola river basin, Florida. J. Hydrol. 480 (4), 125–135.
Wang, G., Wang, D., Trenberth, K., 2017. The peak structure and future changes of the relationships between extreme precipitation and temperature. Nat. Clim. Chang. http://dx.doi.org/10.1038/NCLIMATE3239.
Westra, S., Alexander, L.V., Zwiers, F.W., 2013. Global increasing trends in annual maximum daily precipitation. J. Clim. 26 (11), 7834.
Whan, K., Zscheischler, J., Orth, R., et al., 2015. Impact of soil moisture on extreme maximum temperatures in Europe. Weather Clim. Extrem. 9 (C), 57–67.
Yang, Y., Chen, W., 2007. Application on the reverse cloud model in speech quality evaluation. Voice Technol. 31 (5), 52–55 (in Chinese).
Yu, Z., Li, X., 2015. Recent trends in daily temperature extremes over northeastern China (1960–2011). Quat. Int. 380–381, 35–48.
Zhang, Y., Gao, Z., Pan, Z., et al., 2017. Spatiotemporal variability of extreme temperature frequency and amplitude in China. Atmos. Res. 185, 131–141.
Zhong, K., Zheng, F., Wu, H., et al., 2017. Dynamic changes in temperature extremes and their association with atmospheric circulation patterns in the Songhua River Basin, China. Atmos. Res. 190, 77–88.
Zhou, Y., Ren, G., 2011. Change in extreme temperature event frequency over mainland China, 1961–2008. Clim. Res. 50 (1–2), 125–139.
Zhu, Y., Huang, S., Chang, J., et al., 2016. Spatial–temporal changes in potential evaporation patterns based on the Cloud model and their possible causes. Stoch. Env. Res. Risk A. 1–12.
Zuo, D.P., Xu, Z.X., Wu, W., et al., 2014. Identification of streamflow response to climate change and human activities in the Wei River Basin, China. Water Resour. Manag. 28 (3), 833–851.